Coexistence of tight and loose bundled states in a model of bacterial flagellar dynamics

P. J. A. Janssen and M. D. Graham

Phys. Rev. E **84**, 011910 — Published 14 July 2011

DOI: 10.1103/PhysRevE.84.011910

Coexistence of tight and loose bundled states in a model of bacterial flagellar dynamics

P.J.A. Janssen and M.D. Graham
Dept. of Chemical and Biological Engineering, University of Wisconsin - Madison, 53706 Madison, WI

Many microorganisms propel themselves through their fluid environment by means of multiple rotating flagella that self-organize to form bundles, a process that is complex and poorly understood. In the present work, the bundling behavior of a pair of flexible flagella, each driven by a constant torque motor, is investigated, using a mathematical model incorporating the fluid motion generated by each flagellum as well as the finite flexibility of the flagella. The initial stage of bundling is driven purely by hydrodynamics but the final state of the bundle is determined by a nontrivial balance between hydrodynamics and elasticity. As the flexibility of the flagella increases a regime is found where, depending on initial conditions, one finds bundles that are either tight, with the flagella in mechanical contact, or loose, with the flagella intertwined but not touching. That is, multiple coexisting states of bundling are found. The parameter regime (in terms of flexibility and distance between motors) at which this multiplicity occurs is comparable to the parameters for a number of bacteria.

I. INTRODUCTION

The modes by which microorganisms propel themselves in fluid to sample and respond to their environments are very diverse. Just among flagellated bacteria, the focus of the present work, there are four different flagellar arrangement schemes. *Monotrichous* bacteria have a single flagellum, *lophotrichous* bacteria have a "tuft" of flagella anchored to a small patch of the cell body, *amphitrichous* bacteria have flagella at either "pole" of their bodies and *peritrichous* bacteria have numerous flagella, anchored at random locations around the cell body. When the molecular motors driving the flagella all rotate in the same direction, the flagella dynamically self-organize into bundles and it is these bundles that propel the organism through fluid. In many species of peritrichous bacteria, including *E. coli*, one or more of the molecular motors will occasionally counter-rotate with respect to the others, causing its flagellum to come loose from the bundle. When this occurs, the bacterium tumbles until the motor begins co-rotating, at which time the flagellum is again drawn into the bundle [1]. This "run-and-tumble" behavior is central to chemotaxis.

Presumably, this array of morphologies has evolved because there are selective advantages to different schemes in different environments, but the origin of this diversity is as yet unknown. One reason for this lack of understanding is that the only means of flagellar propulsion whose principles are well-understood is that due to a single flagellum. Therefore, the locomotion of multiflagellar prokaryotes is a frontier problem in the physical biology of microorganisms.

The importance of understanding the mechanics of flagellar propulsion goes beyond biology, however. As nanotechnology advances toward the capability to manufacture microscopic artificial swimming machines (see e. g. [2, 3]), it will be important to understand the principles underlying natural propulsion at the microscale, to determine whether evolution has found solutions that technology should emulate. In other words, we need to know if there is something that biology can teach us about what machines will function best in the various environments encountered by microscale swimmers.

Prokaryotic flagella are slender helical filaments; the net propulsive force exerted by the rotating flagellum originates in the difference in viscous drag due to motion normal to and parallel to the local axis of the filament [4–6]. The hydrodynamic formalism of slender body theory allows a quantitative understanding of this phenomenon [7–9]. In contrast, the issue of interactions *between* flagella lacks a comparable level of mechanistic understanding. This is because of a number of complexities that arise [10]: for bundling to occur, (1) the molecular motors must synchronize, (2) the flagella must approach one another and (3) the geometry and mechanics of the flagella must be such that nearby flagella can properly "mesh" into a stable bundle.

Recent work has led to some understanding of the first two of these issues. Synchronization due to hydrodynamic interaction between objects rotating in fluid has been the subject of substantial recent work [11–15]. In general, synchronization is often observed the presence of phase compliance of the driving mechanism and some mechanical compliance (flexibility) of the rotating objects. The issue of robustness with respect to noise or to detuning of driving torques has not yet been systematically addressed. The initial approach of rotating flagella toward one another can be understood on hydrodynamic grounds, as most clearly illustrated by Kim *et al.* [16], in a study of a macroscopic physical model of a pair of flagella driven by constant speed motors. Flow generated by parallel aligned helices driving fluid axially in the same direction drives fluid motion that tilts each helix toward the other (because the helices draw fluid in radially to pump axially. Additionally, the rotational component of velocity tends to cause the helices to wrap around one another, promoting bundling. Similar observations were made in the computational study of Flores *et al.* [17]. In this study, the bundling of three flagella each driven by a constant torque is studied, and visualizations of the flagellar and fluid motion during the bundling process are provided. Another recent computational study [18] uses a coarse-grained model of a multiflagellar organism to simulate bundling and unbundling in a free swimming cell as well as run-and-tumble dynamics. This work also incorporates stress-induced polymorphism (in particular, the change in pitch and handedness of the *E. coli* flagellum upon clockwise rotation[19–21]). None of these studies systematically addressed synchronization of the motors, the geometry of the flagellar bundle or the parameter dependence of the bundling process. In particular, the final stage of bundling, in which the flagella approach and intertwine, is not understood, but is the most biologically important aspect of the phenomenon. The robustness of bacterial run-and-tumble behavior relies on a delicate balance in the bundling dynamics: if bundles are too tight, counter-rotation of a molecular motor for a fraction of a second will not be sufficient to drive unbundling, but if they are too loose, they will not re-form rapidly and will not be robust to perturbations.

As a first step toward understanding bundling, the present work focuses on the dynamics of a pair of rotating prokaryotic flagella suspended in a viscous fluid (Figure 1). Using a relatively simple mathematical model that captures the elasticity of the flagella as well as the effects of the fluid motions driven by the rotating flagella and the physical contacts between them, we characterize for the first time the entire bundling process, including its dependence on key geometric and dynamical parameters. The results indicate the interplay between geometry, fluid stresses, elastic stresses and physical contacts that determines the final structure of the flagellar bundle. This work thereby provides the foundation for further studies of bundling and for beginning to understand the role that flagellar bundling plays in prokaryotic locomotion.

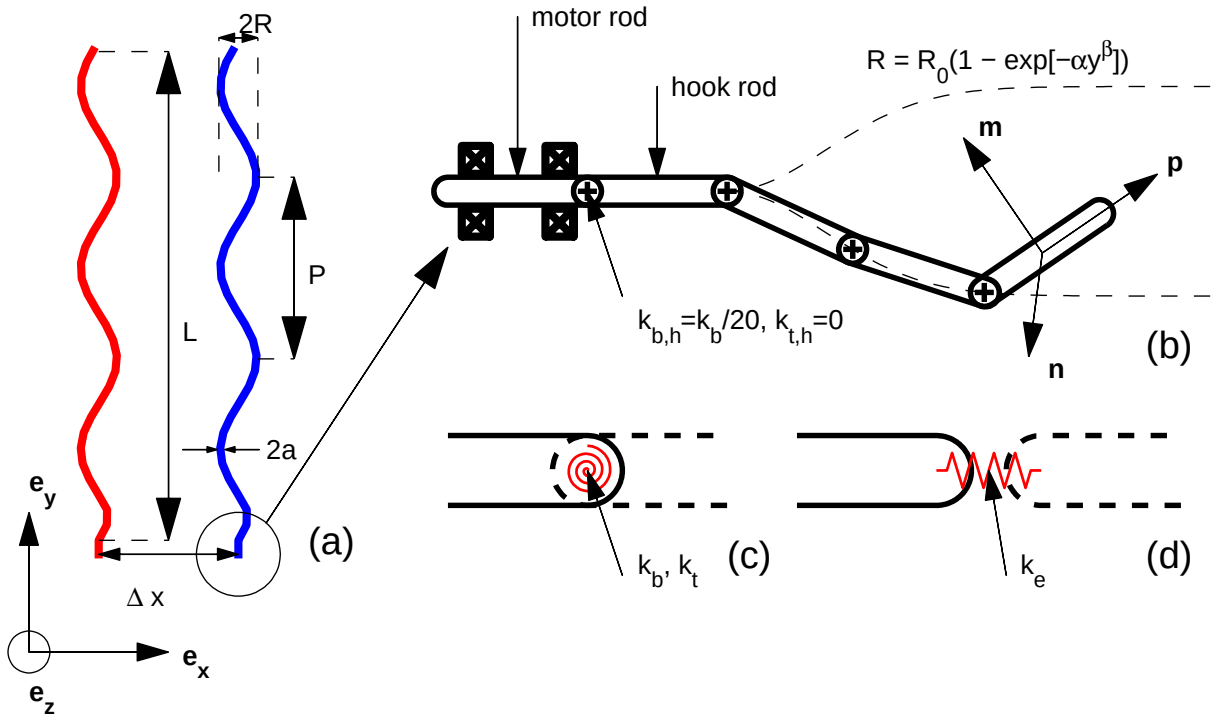

Figure 1. (Color online) (a) Schematic representation of two helices next to each other, showing the relevant length scales. The flagella radii are exaggerated by a factor of 3 for clarity. (b) Detail of the motor region. The motor rod is anchored and has a fixed orientation. The hook rod is free to orient itself relative to the motor rod, except for a small bending potential. The helix radius makes a smooth transition from 0 to R. (c) Detail of connections between rods. In each connection, torsion springs between rods provide resistance to bending and twisting, while (d) extensional springs provide resistance to stretch. Both type of springs are present in all connections.

II. MODEL OF INTERACTING FLAGELLA

We consider the dynamics of two identical left-handed helical flagella placed side by side in an unbounded fluid with viscosity μ, as shown in Figure 1. At first sight, the biological relevance of this configuration seems limited, but for example, a forward swimming motion of a bacterium will have a tendency to align flagella behind the cell. A similar configuration could be found for flagella anchored at a surface.

Each flagellum has a radius a, and at rest takes the shape of a helix with radius R, pitch P and length L. The flagella are each attached to a motor, fixed in space, that exerts a constant counter-clockwise torque T in the y direction. The motors are at positions $(0,0,0)$ and $(\Delta x,0,0)$. The choice of constant torque is based on the observations of Berg and coworkers [22, 23] that for rotation speeds less than about 200 Hz, the torque exerted by *E. coli* molecular motors are indeed nearly constant. (Recall that Flores *et al.* [17] also impose constant torque.) The section of the flagellum closest to the motor is treated as the bacterial hook; it is nearly a universal joint [24], so it has low bending resistance and high twisting resistance. Therefore, each helix is free to point in any direction, but will still be driven by the motor. At rest, the helices point in the y direction. The bending resistance of each helix is given by EI, where E is the Young's modulus and I the area moment of inertia; the twisting resistance is given by GJ with G the shear modulus, and J the polar moment of inertia. The ratio EI/GJ is $3/2$ for an incompressible solid, which we assume here. At the base, the local radius of the helix makes a smooth transition from 0 to R.

The helix radius R is used to scale all other length scales, and time is scaled with $T/(6\pi^2\mu R^3)$, which is an estimate of the rotation period for a circle of radius R made up of spherical particles with radius a and driven by a torque T. Forces are scaled with T/R. Therefore, the dimensionless groups in the problem are the length ratios, the ratio between the bending and twisting resistance $k_b/k_t = EI/GJ$, and the ratio RT/EI between the applied torque and the bending resistance, which we will call the *flexibility number* Fl. This important quantity is related to the sperm number that arises in many other propulsion problems. However, the sperm number contains an actuation frequency or rotation speed, but in the case of bacterial flagella, it is the motor torque that is given [22, 23], not a speed or frequency. Based on biological data for flagella of *E. coli* [25], we choose a helix pitch of $10R$, a helix length of $30R$,

and a flagella radius a of $0.04R$. For *E. coli*, Fl ≈ 0.1 [1, 25, 26]; we will examine the bundling dynamics over a range of Fl.

To simulate the behavior of the flagella, we use a discretized model. Each helix is modeled as an assemblage of N rods with length l and radius a, which are connected at their ends by stiff linear and torsion springs to form a long chain. In this study, for each flagellum we used $N = 32$ rods with length $l = 1.1$ and radius $a = 0.04$. The springs provide resistance to bending, twisting, and extension, so that the helix can deform, but in the absence of external forces and torques will return to the helical shape. Models of this type have been very successful in representing the dynamics of suspensions of flexible fibers [27]. A related of model consisting of spheres connected by long springs was recently used to simulate the run-and-tumble motion of a bacteria [18].

The modeling of the hook and motor requires special attention. The first rod is anchored in space, and is labeled the motor rod. Its only function is to exert a constant torque on the second rod, the hook rod, with magnitude T and direction $\mathbf{e}_y$. The hook in a prokaryotic flagellum is a semi-flexible connection, having properties reminiscent of a universal joint, i.e. low bending and high twisting resistance. Because in our model, the torque generated by the motor is directly passed to the hook rod, no twisting potential has to be taken into account between the motor and hook rods ($k_{\text{twist,hook}} = GJ/l = 0$. The bending potential in this connection is taken to be 20 times lower than in the rest of the chain, to simulate the universal joint characteristic of the hook ($k_{\text{bend,hook}} = EI/l = 0.05$). The motor rod is still needed to provide an orientation vector for this bending potential, as well as a tip location for the extensional springs. The bending and twisting constant in all the other joints are 1 and 2/3, respectively. The motor rod is always oriented in the y direction and at equilibrium the hook rod is as well. To get a smooth transition from the hook rod to a helical shape, the other rods are placed on a cylinder with varying radius: $R = R_0\left(1 - \exp\left[-\alpha y^{\beta}\right]\right)$, where y runs along the helix length, and α and β can be tuned. Here, $\alpha = 1$ and $\beta = 2$. A schematic representation is given in Figure 1.

The role of Brownian forces in flagellar shape can be addressed by considering the persistence length of a flagellum. Based on the flexural rigidity $EI = 3.5 \cdot 10^{-24} Nm^2$ of an *E. coli* flagellum [26], we estimate its persistence length as $\sim 0.7mm$. Because the persistence length of a flagellum is so much larger than its contour length (about $10\mu m$), it is justifiable to neglect the effects of thermal fluctuations on flagellar shape. We can also estimate the importance of Brownian motion for flagellar dynamics. For a flagellum of helical radius $R = 0.2\mu m$, rotating at 100 Hz, its rotational velocity U is about $125\mu m/s$. Estimating the translational diffusivity of a flagellum as $D = 1\mu m^2/s$ yields a Péclet number UR/D of about 125; this large value indicates that the motor-driven motion of the flagella dominates over Brownian motion and indicates that the latter can be safely neglected when considering bundling dynamics. Based on these analyses, Brownian motion is not included in our formulation.

III. GOVERNING EQUATIONS

The equations of motion of each rod are generated by balancing the applied forces and torques with the hydrodynamic resistance to translation and rotation respectively; because of the small scale of bacterial flagella, both fluid and solid inertia are neglected. Each rod i is described by a mass center $\mathbf{r}_i$, and three orthonormal orientation vectors $\mathbf{m}_i$, $\mathbf{n}_i$, and $\mathbf{p}_i$, where the latter runs along the length of the body (see Figure 1b). The forces acting on an individual rod include the spring forces and forces due to contact with other rods; the torques include bending and twisting resistance, torques due to forces not applied in the mass center, and in the case of the hook rod, the applied motor torque. For determining hydrodynamic resistance, the bodies are considered to be prolate spheroids [28]; to determine contact, they are considered rods with hemispherical caps, and for hydrodynamic interactions, they are modeled as smoothed point forces.

The equations of motions for the position $\mathbf{r}_i$ and angular velocity $\boldsymbol{\omega}_i$ of each rod are:

$$\dot{\mathbf{r}}_i = 2\pi \frac{R}{l} \mathbf{A}_i^{-1} \cdot \left(\sum \mathbf{F}_i\right) + \frac{3\pi}{4} \sum_j \boldsymbol{\Omega}_{ij} \mathbf{F}_j, \tag{1}$$

$$\boldsymbol{\omega}_i = 6\pi \left(\frac{R}{l}\right)^3 \mathbf{C}_i^{-1} \cdot \left(\sum \mathbf{T}_i\right). \tag{2}$$

The second term in the right-hand side of Equation (1) represents the hydrodynamic interaction between the rods in the form of regularized Stokeslets, discussed below. The tensors $\mathbf{A}$ and $\mathbf{C}$ are the hydrodynamic resistances of prolate

spheroids [28], where the prefactors have been scaled out:

$$\mathbf{A}_i^{-1} = \frac{1}{Y^a}\mathbf{I} + \left(\frac{1}{X^a} - \frac{1}{Y^a}\right)\mathbf{p}_i\mathbf{p}_i, \tag{3}$$

$$\mathbf{C}_i^{-1} = \frac{1}{Y^c}\mathbf{I} + \left(\frac{1}{X^c} - \frac{1}{Y^c}\right)\mathbf{p}_i\mathbf{p}_i, \tag{4}$$

with $\mathbf{p}$ the orientation vector running along the rod length. The resistance parameters X^a, Y^a, X^c, and Y^c are functions of the dimensionions of the spheroids, and can be found elsewhere [28]. In our case, with $a = 0.04$ and $l = 1.1$, these values are $X^a = 0.1078$, $Y^a = 0.1856$, $X^c = 4.167.10^{-6}$, and $Y^c = 0.0539$. The forces $\mathbf{F}_i$ acting on the rods consist of the spring forces $\mathbf{F}_{\text{spring},i}$ and $\mathbf{F}_{\text{spring},i+1}$, who act against the extension of the flagellum, as well as all the contact forces $\mathbf{F}_{\text{contact}}$ acting on the rod:

$$\sum \mathbf{F}_i = \mathbf{F}_{\text{spring},i+1} - \mathbf{F}_{\text{spring},i} + \sum \mathbf{F}_{\text{contact}}. \tag{5}$$

The spring forces $\mathbf{F}$ are proportional to the distance between the tips of two consecutive rods:

$$\mathbf{F}_{\text{spring},i} = k_e\left(\mathbf{r}_{i+1} - \mathbf{r}_i - \frac{l}{2R}\left(\mathbf{p}_i + \mathbf{p}_{i+1}\right)\right) \tag{6}$$

with $k_e = 200$ here (see Figure 1d) – i.e. they are very stiff and keep the flagellar length constant to within 0.1%. Contributions to the torque $\mathbf{T}_i$ include the torsion springs in the joints, as well as torques generated by forces not acting in the mass center:

$$\begin{aligned}\sum \mathbf{T}_i = {} & \frac{R}{l}\mathrm{Fl}^{-1}\left(\mathbf{T}_{\text{torsion},i+1} - \mathbf{T}_{\text{torsion},i}\right) + \frac{l}{2R}\mathbf{p}_i \times \left(\mathbf{F}_{\text{spring},i} + \mathbf{F}_{\text{spring},i+1}\right) \\ & + \sum \mathbf{b} \times \mathbf{F}_{\text{contact}}.\end{aligned} \tag{7}$$

The arm $\mathbf{b}$ is proportional to $\mathbf{p}$ and runs from the mass center of the rod to the location of minimal contact with the other rod. The proportionality factor can be positive or negative and has a maximum absolute value of $l/2R$. Details on computing the location of the minimal contact, as well as expressions for $\mathbf{T}_{\text{torsion}}$, which includes bending and twisting resistance, are in [27]. The sum over the contact forces and torques indicate that one rod can be in contact with multiple other rods. The contact force between two rods is $120\exp\left[-20(d-2a)/a\right]$, where d is the minimal distance between the rod center lines. The hook rod has an additional contribution $\mathbf{e}_y$ to the torque, which is the driving torque of the motor (the magnitude T has been scaled out).

Hydrodynamic interactions between flagellar segments are incorporated via a Stokeslet $\mathbf{\Omega}_{ij}$, regularized so no rod can generate a velocity larger than its own speed [29]:

$$\mathbf{\Omega}_{ij} = \mathbf{\Omega}\left(\mathbf{r}_{ij}\right) = \left(\mathbf{I} + \frac{\mathbf{r}_{ij}\mathbf{r}_{ij}}{r_{ij}^2}\right)\frac{\mathrm{erf}\left(\xi r_{ij}\right)}{r_{ij}} + \left(\mathbf{I} - \frac{\mathbf{r}_{ij}\mathbf{r}_{ij}}{r_{ij}^2}\right)\frac{2\xi}{\pi^{1/2}}e^{-\xi^2 r_{ij}^2}, \tag{8}$$

with $\xi = 2\sqrt{\pi}/(3lY^a)$; ξ^{-1} is the length scale for the regularization. The vector $\mathbf{r}_{ij}$ is the vector between the mass centers of rods i and j, and r_{ij} is the length of this vector. This is in effect a discretized slender-body treatment of the hydrodynamic interactions between segments, as is widely used in the analysis of flagellar motion [7, 8]. This treatment does not include near-field lubrication interactions between flagella approaching contact, but Sundararajakumar and Koch [30] have shown that these are negligible in the case of large aspect ratio filaments that we consider here.

Time integration is conducted with an Adams-Bashforth scheme. To avoid numerical instabilities associated with the restoring torques, it is necessary to take a time step of the order of 10^{-5}. The most expensive computation done at each time step is the computation of $\mathbf{\Omega}_{ij}$ for each rod-rod combination. Because these are only a function of position, and the time step is so small, we only compute $\mathbf{\Omega}_{ij}$ once every 50 time steps and assume it is constant during this period. This approximation results in negligible error and significantly decreases the total computation time required.

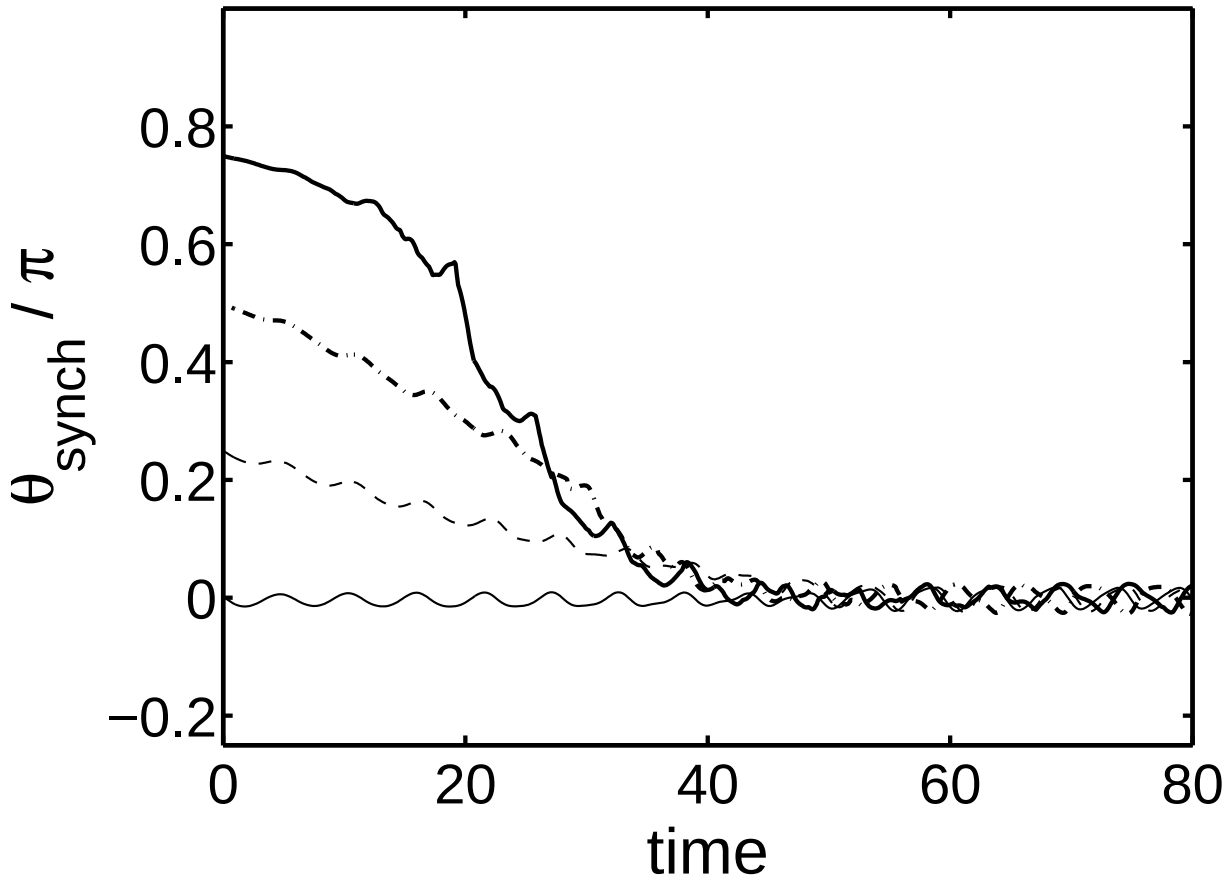

Figure 2. The synchronization angle between the hook rods of two flagella with Fl = 0.1 and $\Delta x = 2.5$ for four different initial angles.

IV. RESULTS

We begin this section by showing in some detail how two flagella come together to form a bundle. With this information as background, we then systematically examine the dependence of the bundling dynamics on the motor spacing Δx and flexibility number Fl. Finally, connections are drawn between the present results and observations in bacteria. Due to the rotational nature of the problem in addition to the discretization of the helices into rods, small fluctuations in time can be seen for certain parameters in time. When stationary values are reported, we average over 100 time units in the long-time region.

A. Synchronization

Before we focus on the details of the bundling, we first discuss synchronization. We take two helices next to each other with Fl = 0.1 and $\Delta x = 2.5$. One of the helices is rotated around the y axis. We then define the synchronization angle as $\theta_{\text{synch}} = \cos^{-1}(\mathbf{m}_{h,1} \cdot \mathbf{m}_{h,2})$, where $\mathbf{m}_{h,1}$ is one of the orientation vectors of the hook rod; the numerical index refers to the specific flagellum. The orientation angle in time for four different initial rotations are shown in Figure 2. The angle does not become perfectly 0, because the flagella both slightly tilt towards each other, and thus the vectors cannot become perfectly parallel. What is important to note is that the synchronization occurs relatively quickly: in 40 or 50 time units the helices are synchronized. This is a relatively short time scale compared with the full bundling dynamics as shown below.

B. Bundle formation

To illustrate a typical bundling case, we focus on two flagella with Fl = 0.1 and an initial separation $\Delta x = 2R$. At the start of the simulation, all flagella are synchronized (in the same rotational orientation with one another). When flagella are not initially synchronized, we find that synchronization occurs rapidly (within about 10 or fewer rotation periods) compared with the bundling dynamics, and is robust versus variation in parameters– therefore we do not focus on it here. Images of the helices at various times during bundling are shown in Figure 3. The motor torques are turned on at $t = 0$ (a), and initially, the two helices deflect only in the z direction (b). Then the flagella begin to wrap around each other (c). Due to the fixed position of the motor rod, they eventually cross, and contact will be made roughly halfway between the base and the tip (d). From that location to the tip, the flagella continue to wrap around each other (e&f), eventually reaching a time-periodic bundled state. The initial stage of the bundling process ($t \lesssim 200$) is quite robust and driven solely by the fluid motion generated by the rotating flagella. The later stage ($t \gtrsim 200$) is much more delicate, depending sensitively on the parameters of the system. We examine the details of these stages in turn.

First, we focus on the initial deflection. In Figure 4, the x and z components of the separation in time between the tips of the two flagella d_{tip} are shown. In the first several time time units, very little happens, as the helices are tightening. As time progresses, initially only the z-deflection increases, but the x-deflection slowly catches up. As the helix tips continue to rotate around each other, their x and z coordinates reach maxima and minima, and eventually a bundled state is reached. Rigid contact between the flagella may occur, depending on the Δx and Fl, but is not a necessity. This is discussed in more detail below. After bundling, the helices still rotate of course, so the absolute x and z coordinates of the tips make a nearly circular motion in time, but the scalar distance between the tips changes very little in time. We denote this final stage of bundling as "stationary."

It is important to note that in the absence of hydrodynamic interaction, no bundle will form. Therefore, the reason for bundling needs to be sought in hydrodynamic interactions between flagella. To explain the initial formation of the bundle, we look at the time-averaged velocity field produced by a single rotating helix. Figure 5b shows the xz projection of this velocity field at $y = 20$. This field is reminiscent of the summation of a velocity field produced by a point torque (rotlet) and that of a sink. The rotlet part comes from the rotating helix, while the sink part comes from the axial pumping motion the rotating helix generates; by continuity, this axial motion needs to be balanced with fluid dragged in to the center of the helix. The rotlet interactions will rotate the helices around each other, but due to the anchoring at the base, the helices will in fact be tilted up and down. When summing two helices next to each other, as depicted in Figure 5c, we see that the sink effects more or less cancel each other out between the helices, and one large rotlet flow remains. From Figure 4, we see that the helices first deflect in the z direction, and not the x direction. Therefore we conclude that the rotlet interactions start the bundling process, and not the sinks. This mechanism is schematically represented in Figure 5a. This behavior is robust in all parameters considered: variations in helix length, separation and stiffness all show similar behavior. It is also consistent with experimental observations of a macroscopic model of hydrodynamically helices by Kim et al. [16].

To more quantitatively characterize bundling, we introduce two quantities: the local distance between the helices d and the bundle angle ϕ_b, defined as the angle that the connector vector between the flagella in an xz cross section makes with the connector vector at the base of the helix. A value of $\phi_b = 2\pi$ at the tip would indicate that the helices have wrapped once around each other. These quantities are shown in Figure 6 for the case shown in Figure 3. The initial nonmonotonic dependence of $d(y)$ on y is due to the initial deflection and eventual crossing of the helices. The location of the minimum distance between the flagella moves in time along the helix length. In the final stationary situation, it is fairly constant over the last part of the helix, showing a small increase at the tip. The minimum distance is the separation at which mechanical contact occurs ($d \approx 0.1$). The bundling angle ϕ_b starts at 0, and increases in time and over the helix length. In the final stationary state, ϕ_b increases nearly linearly over most of the helix, and the helices do not wrap a full 2π radians around each other. The potential biological significance of this result is discussed below.

C. Parameter dependence: multiplicity

We now turn to the dependence of the bundling dynamics on the key geometric and mechanical parameters Δx and Fl. To begin, we show in Figure 7 the time evolution of d_{tip} and ϕ_b for several different motor rod separations Δx. Flagella closer together bundle faster, as indicated by the trends: d_{tip} decreases earlier in time, and ϕ_b increases more rapidly. While the final tip distance is practically identical for the flagella closer together, the bundling angle is larger – they wrap more around each other.

A key observation from Figure 7 is that when $\Delta x = 1.5,\ 2$ or 2.5, $d_{\text{tip}} \approx 0.1$ – the flagella are in contact. On the other hand, when Δx is increased to 3, d_{tip} increases sharply to about 0.7, and examination of the entire distance

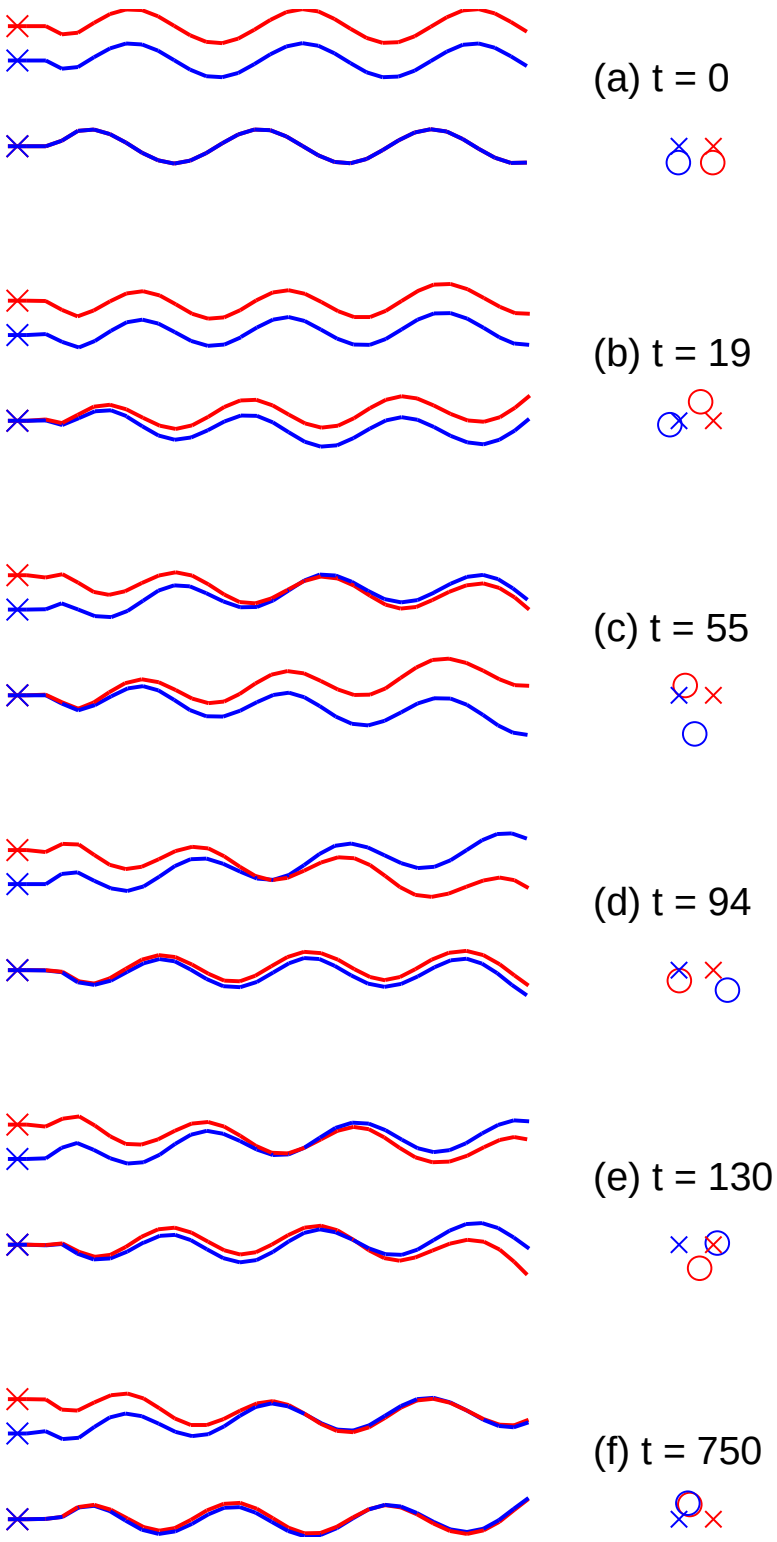

Figure 3. (Color online) Images of two bundling flagella in time with Fl = 0.1 and $\Delta x = 2$. The top picture is looking in the xy plane, the bottom picture is in the yz plane. The circles on the side represent the mass centers of the last rod in the xz plane, looking from the back of the helix towards the anchor points, while the crosses denote the locations of the anchor points. The images correspond to maxima and minima in Figure 4, where they are indicated as well. The flagella radii are exaggerated by a factor of 3 for clarity.

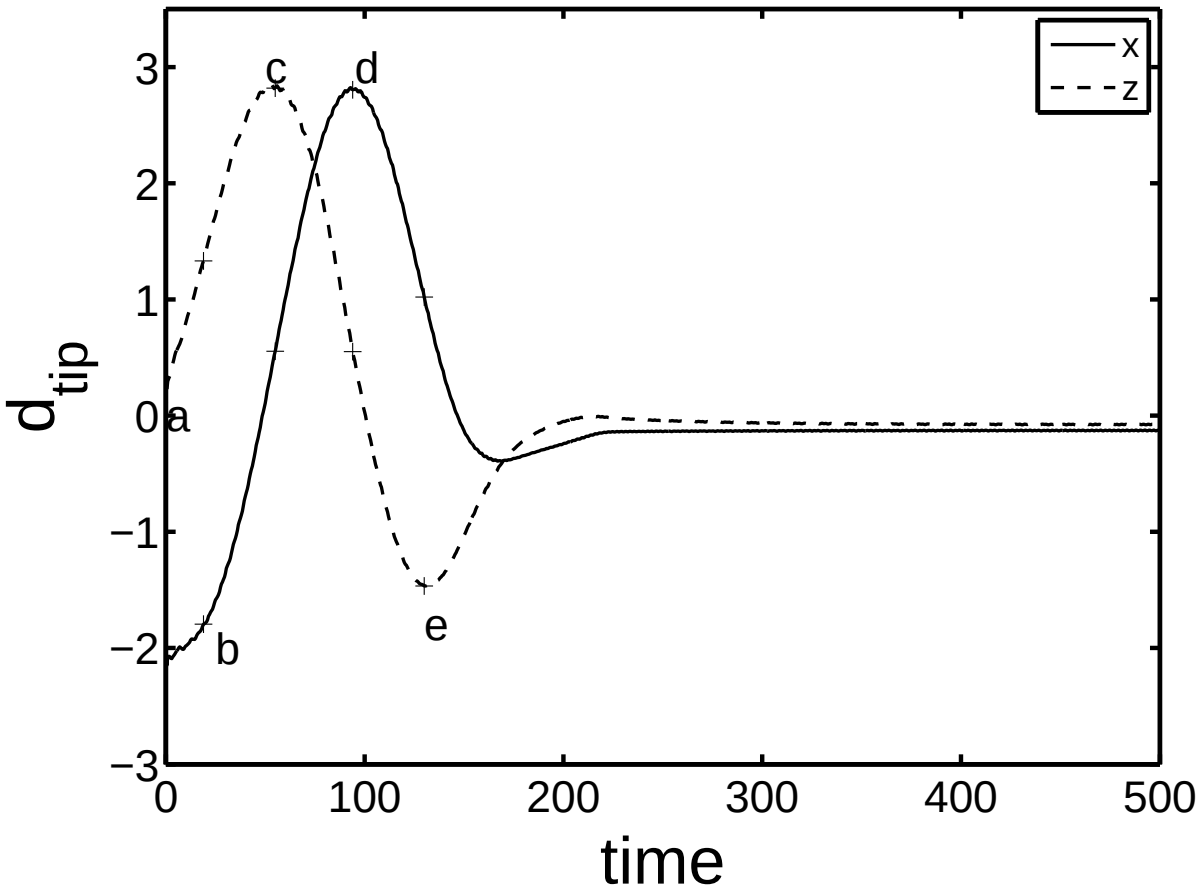

Figure 4. The x and z coordinates of the distance between the two last rods of each flagella *vs.* time with Fl = 0.1 and $\Delta x = 2$. The letters correspond with the images in Figure 3.

profile $d(y)$ reveals that the flagella are no longer in mechanical contact at all, although they are still "bundled" in the sense of being wrapped around one another, less than a radius apart and moving in synchrony.

To generalize this observation, Figure 8 shows the long time values of the minimal distance between the flagella over the whole helix length $d_{\min,\text{helix}}$, as well as the bundle angle ϕ_b at the tip as function of the base separation Δx and Fl. The minimal distance over the helix length was used instead of the tip distance, because it is a better measure to quantify if helices are in contact or not. These plots clearly indicate that for significantly flexible flagella multiple stable bundled conformations are possible. We now describe this figure in further detail. Using completely unbundled states as initial conditions, we can clearly observe two different trends for all Fl. For small Δx, the flagella in the stationary situations are very close to each other, at a distance at which repulsive forces become important: i. e they are in contact. However, for larger motor rod separation, $d_{\min}$ is significantly larger – the flagella are no longer in contact. Besides the large increase in d, the bundling angle also makes a significant drop, as shown in Figure 8b. The most interesting aspect of the difference is that the transition is not smooth, but very sharp and sudden when starting from completely unbundled states. For Fl = 0.1, the transition point is at about $\Delta x = 2.6$. We label these bundles as "tight" and "loose".

Now, instead of using unbundled initial conditions, consider the case where make incremental changes in the motor rod distance, each time starting from a stationary situation with a slightly larger or smaller motor rod distance. Now we see that overlapping solution branches emerge: one for tight and one for loose bundles. Which solution branch is observed depends on initial conditions. In other words, for a window in motor rod separations (for Fl = 0.1: $2.325 < \Delta x < 2.85$) there exist two stable stationary states for the same motor rod separation. This coexistence window grows with increasing Fl. Coexisting stable tight and loose bundles are shown in Figure 9.

The origin of this multiplicity lies in the nonlinear competition between the hydrodynamic interactions between flagella, which promotes bundling as shown in the previous section, and the elasticity of the flagella, which resists the deformations that are required for the two flagella to mesh into a single bundle. In particular, the hydrodynamic

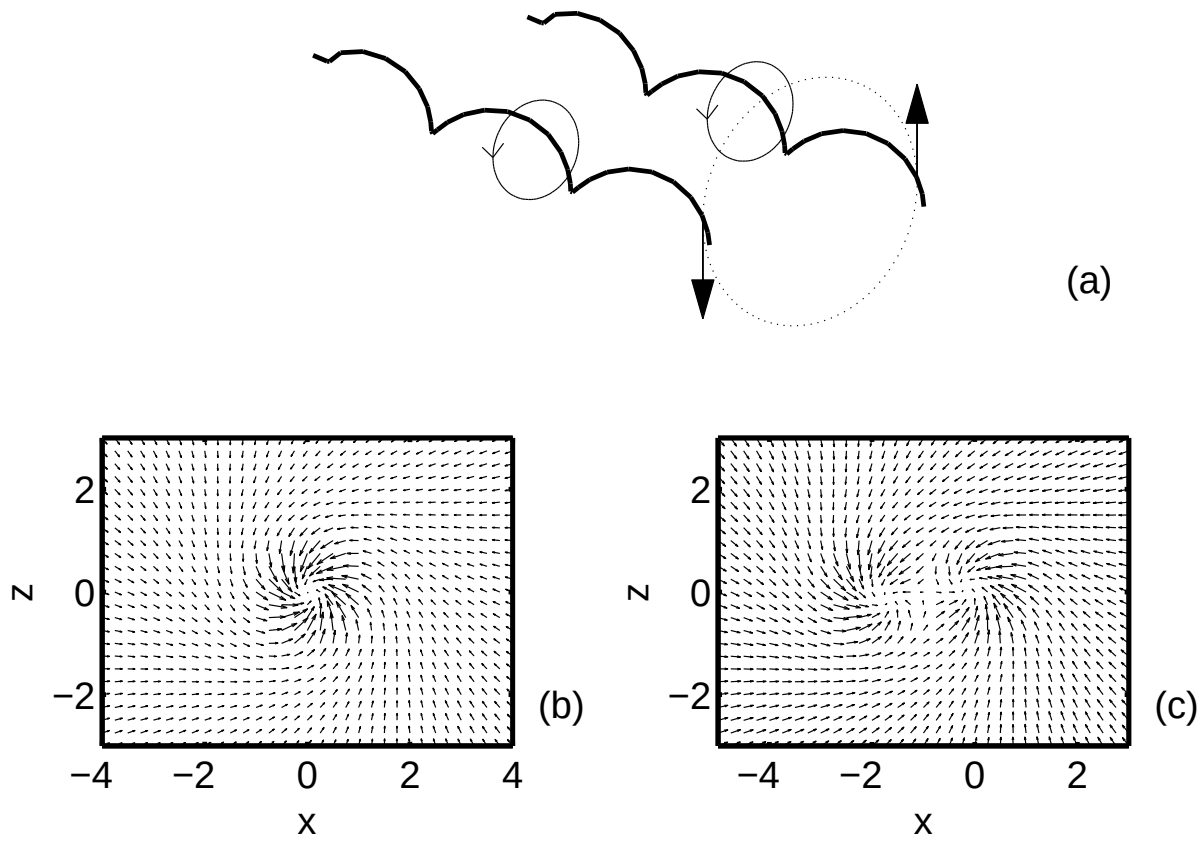

Figure 5. (a) Rotlet interaction between the two rotating helices tilts the helices in opposite z direction. Combined with the anchoring, this ensures that the bundle formation starts. (b) The time-averaged velocity field produced by a single helix projected in the xz plane while looking from the end of the helix to the anchor points. (c) Summation of the velocity field of (b) and the same field, but shifted with $\Delta x = 2$.

interactions between flagellar segments are strongly nonlinear, decaying as $1/r$ where r is the distance between segments. It is important to note that the geometric contact between flagella in a bundle is insufficient to maintain bundling – if we generate a tight bundle, then turn off the hydrodynamic interactions, the bundle will immediately loosen and eventually disintegrate.

The model system considered here is of course much simpler than a real bacterium. Nevertheless, some of the observations may have relevance with regard to parameter regime in which bacteria have evolved to operate. Consider first the observation that the tip bundling angle $\phi_{b,\mathrm{tip}}$ is a decreasing function of the motor separation Δx. If the bundle angle is very large, then the flagella are highly intertwined, a situation that is not conducive to the rapid unbundling that is required for a bacterium to execute a tumbling motion. Therefore, one expects that situations with very closely spaced flagella would not be commonly observed in bacteria that run and tumble. On the other hand, we observed that when Δx is large, tight bundles do not form at all. In the multiplicity regime, in most cases the tight branch is reached when starting from an unbundled state – except at the upper end of the multiplicity regime accessing the loose branch usually requires starting from initial conditions that are close to a loosely bundled state. This can be seen from Figure 8a, where for all Fl the dashed part of the loose branch is longer than the dashed part of the tight branch (between the two small symbols below the curve). Furthermore, we have found that if the motors are turned off, a tightly bundled state will take longer to fall apart than a loosely bundled state with the same Δx. The conclusion we draw from these observations is that for the parameter space investigated in this study, tight bundles are more robust. Whether this statement can be generalized to more complicated and realistic flagellar schemes remains to be investigated. Assuming that tight bundles are desirable from the point of view of robustness but that a very large bundling angle is undesirable, one then expects that run and tumble bacteria will operate with motor separation just below or inside the multiplicity regime.

To further address this issue, we show in Table I data on cell diameter D (as an approximate measure of motor rod separation) and helix radius R for seven species of peritrichous bacteria. Averaged over these species, the ratio $D/R \approx 3.3$. This gives a rough estimate of Δx for these species. Data is not available to determine the flexibility

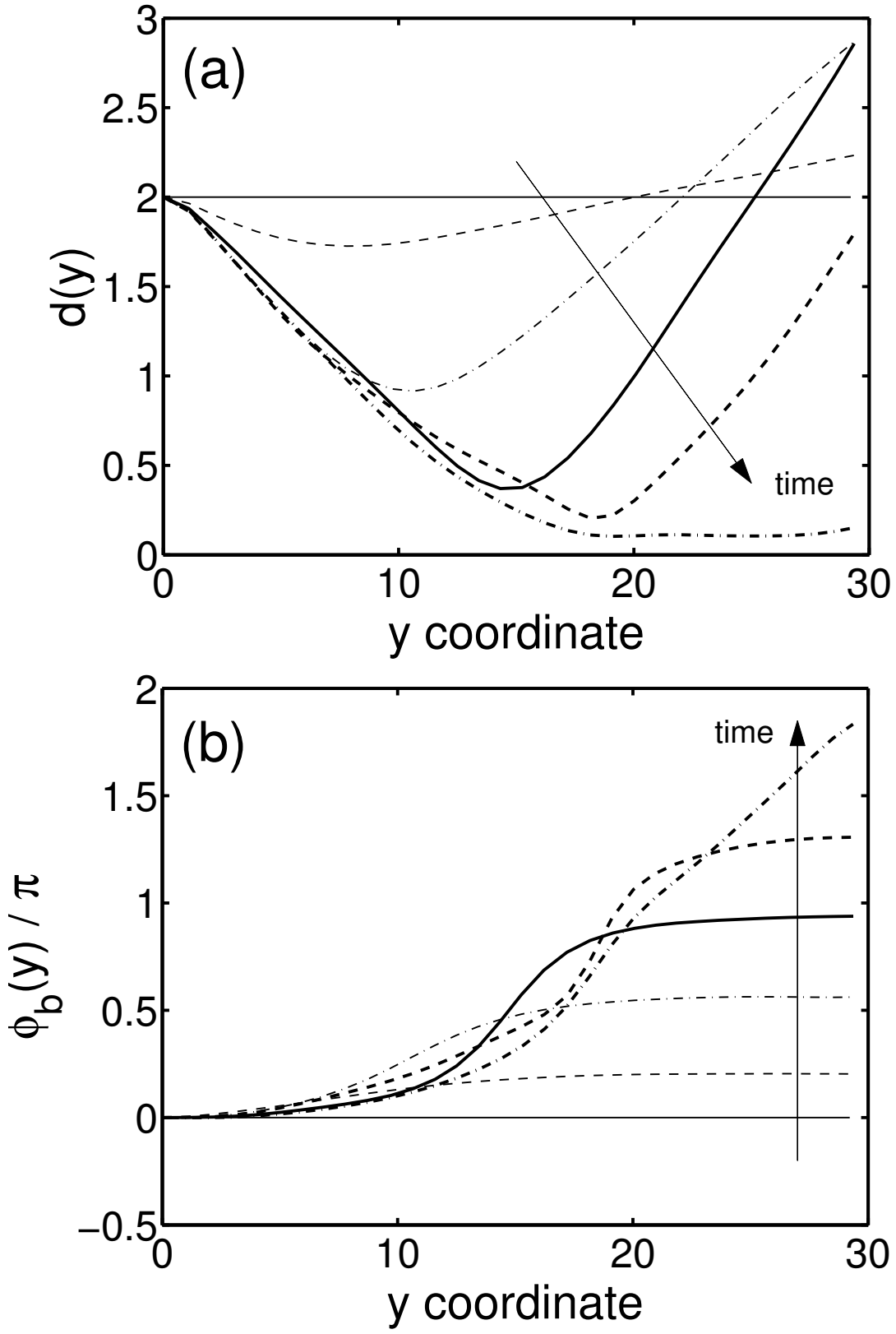

Figure 6. The local distance (a), and local bundle angle (b) between the rods making up the flagella as function of the y coordinate at various instances in time, corresponding with those in Figure 3. $\mathrm{Fl} = 0.1$ and $\Delta x = 2$.

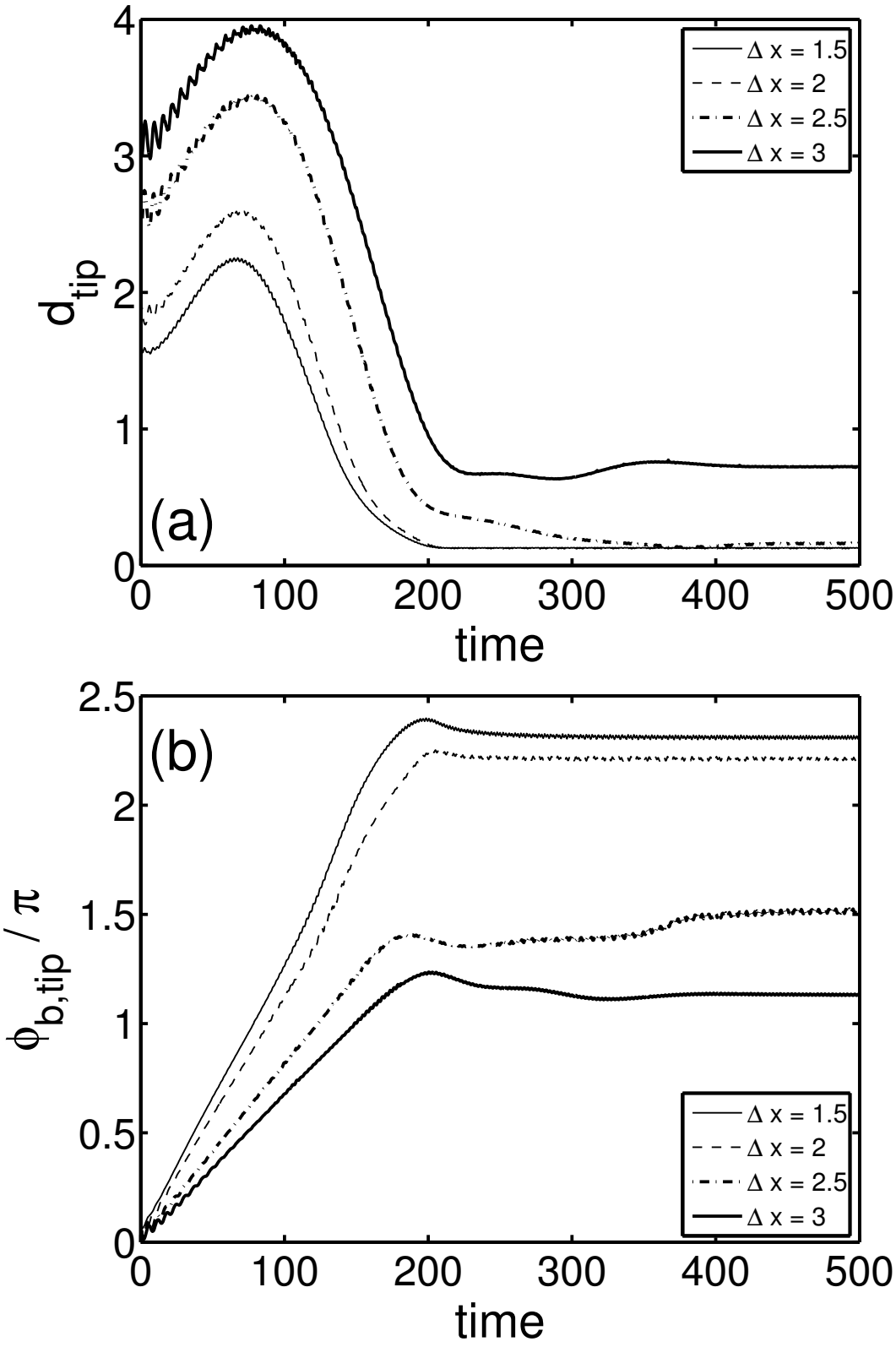

Figure 7. a.) The tip distance in time for multiple motor rod separations with Fl = 0.1. b.) The bundling angle.

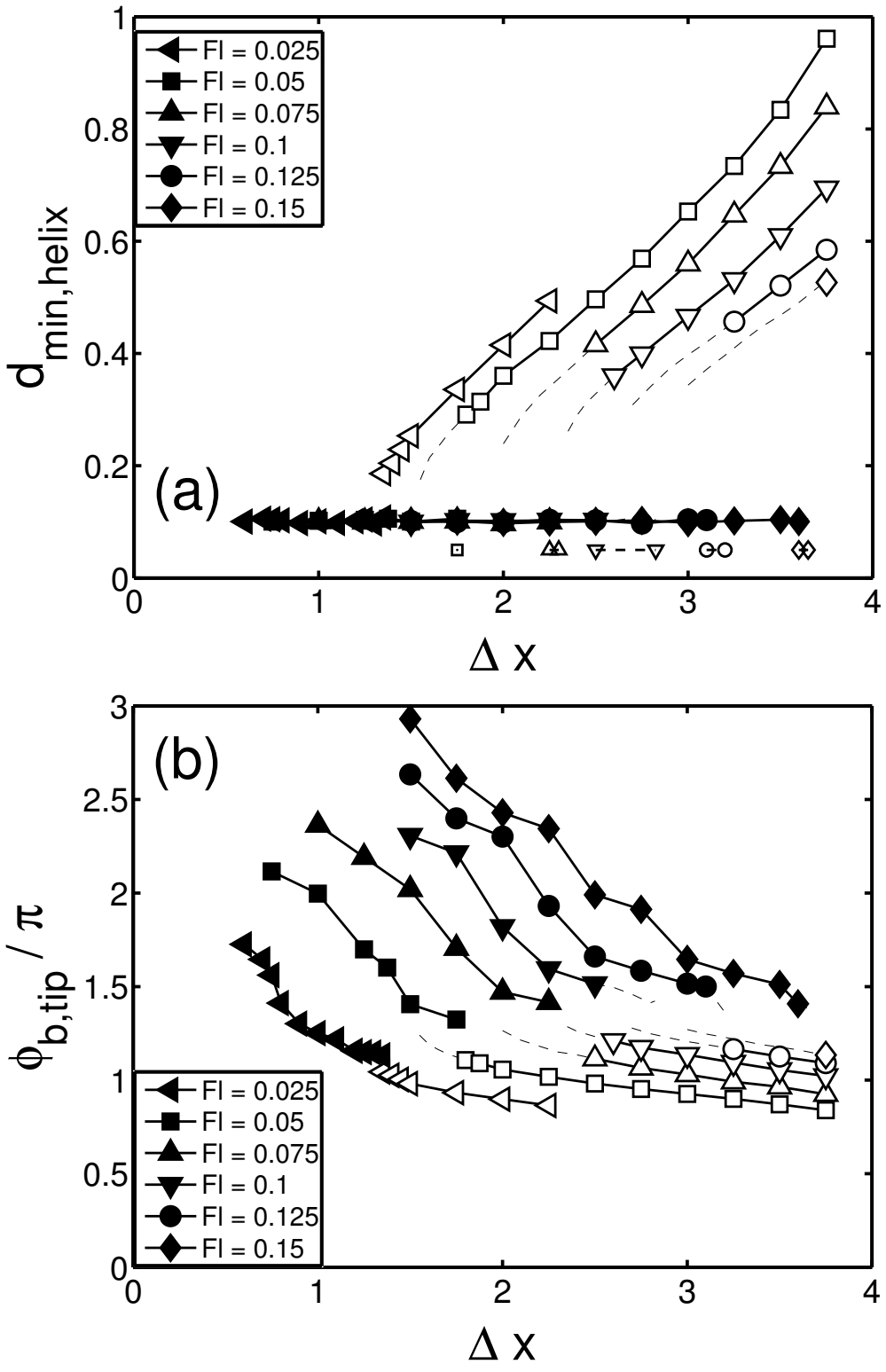

Figure 8. (a.) The time-averaged minimum distance between the flagella and (b) bundling angle at the tip in stationary situations as functions of the motor rod separation for multiple Fl. b.) The dashed parts of the branches were reached by making incremental steps in the anchor distance, starting from a bundled state. For the tip distance, this part of the branch is further indicated with the smaller dashed line between the symbols below the curves. The filled symbols refer to a tightly bundled state, whereas the open symbols represent loose bundles.

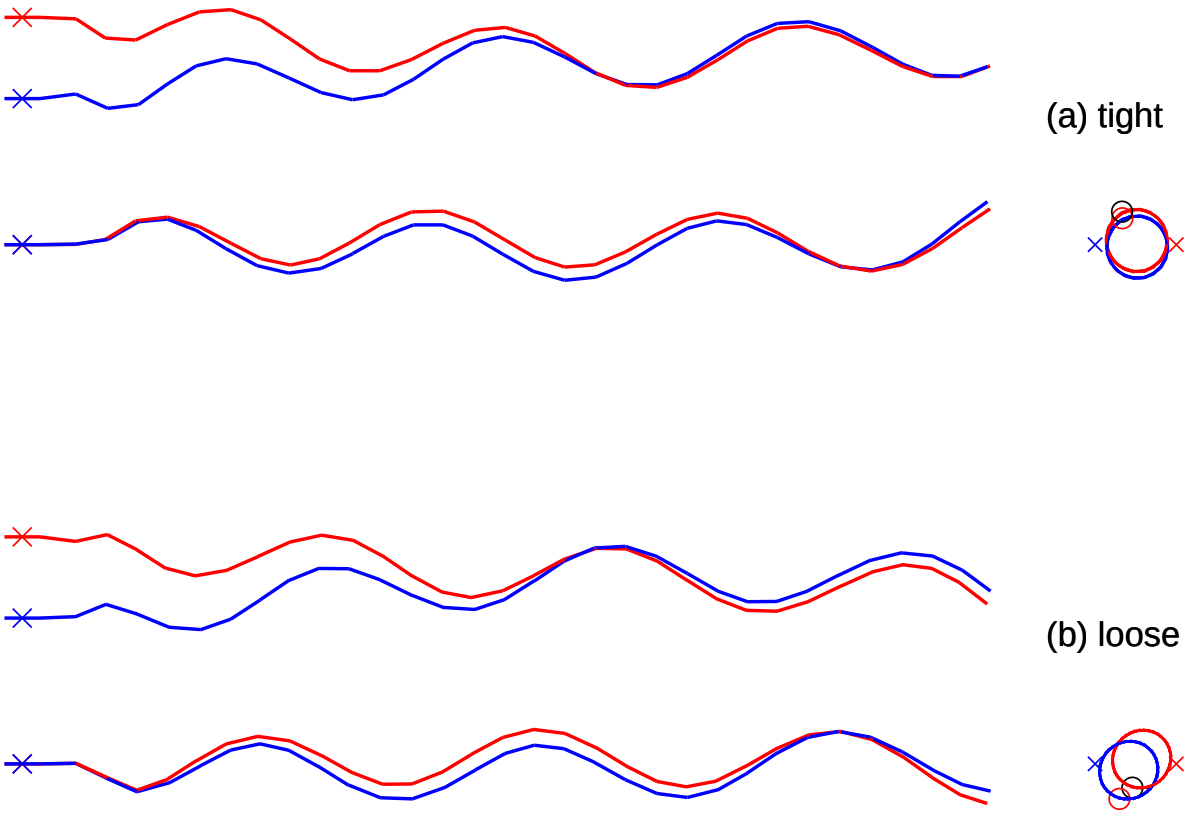

Figure 9. (Color online) Snapshots of tight (a) and loose (b) bundles, both with Fl = 0.1 and $\Delta x = 2.5$. The tight bundle was generated by starting from a completely unbundled situation, while the initial condition for the loose bundle was a loose bundle at $\Delta x = 2.6$, after which the motor rods were slowly moved to $\Delta x = 2.5$. In the xz projections on the lower right of each figure, the crosses represents the locations of the motors, the lines track the locations of the tips for a limited time period, and the circles donate the locations of the tips at the end of this period.

Table I. Cell diameter D and helix ratio R of several peritrichous bacteria. Helix data from [31], cell data from [32].

species	$D[\mu m]$	$R[\mu m]$	D/R
Bacillus subtilis	0.75	0.21	3.6
Enterococcus faecalis	0.9	0.25	3.6
Erwinia carotovora	0.75	0.28	2.6
Escherichia coli	0.8	0.21	3.9
Proteus mirabilis	0.6	0.24	2.5
Salmonella typhimurium	1.1	0.3	3.7
Yersinia enterocolitica	0.9	0.28	3.3
mean values	0.83	0.25	3.3

number Fl for all these species, but over the range of Fl considered here, which we believe to be biologically reasonable, the lower end of the multiplicity regime, as seen in Figure 8, is in the range $1.5 \lesssim \Delta x \lesssim 3$. Thus we have reasonable agreement between the lower end of the multiplicity regime and the parameter regime in which peritrichous bacteria are found. This correspondence does suggest that a relationship exists between the nonlinear dynamics of the bundling process and the selection of cell morphology. Nevertheless, further study is clearly needed. In particular, both the effect of counterrotation of the cell body and the dynamics of unbundling must be addressed in more detail. In the present model, simply reversing the direction of one motor of a bundle leads in many cases to jamming, so it may be that polymorphism is required for a robust smooth escape of an individual flagellum from the bundle, as has been suggested in the literature [10].

Finally, we touch on the issue of the propulsion efficiency of flagellar bundles. In the present case, two isolated flagella produce in sum about 40% more thrust than a bundled pair – bundling decreases thrust. The difference between tight and loose bundles is about 4% (loose bundles provide more thrust). This result is qualitatively consistent with estimates of Darnton *et al.* [26]: flagellar bundling does not confer any propulsive advantage to bacteria.

V. CONCLUSIONS

This work realistically and systematically considers the geometry and elasticity of flagella simultaneously with the mechanism of flagellar bundling. It reveals that the bundling phenomenon has a rich dynamical landscape that includes the possibility of multiple states of bundling arising for the same geometric and mechanical properties and driving forces. The potential biological benefits and drawbacks of the different states remain unclear at the moment, but we speculate that they are related to the dynamic interplay between the ability to form a tight bundle, as well as the need to unbundle. The results described here can be directly compared with experiments on macroscopic physical model systems - indeed, related models are beginning to be studied [14, 16].

The model used here will serve as a testbed for future studies of a variety of important problems in bacterial locomotion, including the flagellar dynamics on free-swimming organisms; the robustness of bundling and locomotion in the presence of stochasticity – especially the random nature of the number and spatial distribution of flagella on a cell; role of stress-induced polymorphism on cell and bundle dynamics, in particular in the unbundling phase; the possibility and consequences of intercellular bundling in dense populations of bacteria [33]; and the role of flagella-driven fluid transport in how cells sense their environments. Additionally, it serves as a starting point for quantitative treatments not just of flagellar motion but also of the dynamics of molecular motors [34, 35] as well as the chemotaxis pathway – it is the coupling of all of these processes that determines the ultimate locomotion behavior of a microorganism.

VI. ACKNOWLEDGMENTS

This work was supported by the National Science Foundation, grant # CBET-0754573. Additional support from the Institute for Mathematics and its Applications with funds provided by the National Science Foundation is gratefully acknowledged as well. The authors also thank Douglas B. Weibel for many helpful discussions.

[1] H. C. Berg, E. coli *in motion* (Springer, New York, 2004).
[2] R. Dreyfus, J. Baudry, M. L. Roper, M. Fermigier, H. A. Stone, and J. Bibette, Nature **437**, 862 (2005).
[3] L. Zhang, J. J. Abbott, L. Dong, B. E. Kratochvil, D. Bell, and B. J. Nelson, Appl. Phys. Lett. **94**, 064107 (2009).
[4] G. J. Hancock, Proc. R. Soc. Lon. Ser. A **217**, 96 (1953).
[5] J. Gray and G. J. Hancock, J. Exp. Biol. **32**, 802 (1955).
[6] M. E. J. Holwill and R. E. Burge, Arch. Biochem. Biophys. **101**, 249 (1963).
[7] J. Lighthill, SIAM Review **18**, 161 (1976).
[8] J. B. Keller and S. I. Rubinow, Biophys. J. **16**, 151 (1976).
[9] S. Chattopadhyay, R. Moldovan, C. Yeung, and X. L. Wu, P. Natl. Acad. Sci. USA **103**, 13712 (2006).
[10] R. M. Macnab, P. Natl. Acad. Sci. USA **74**, 221 (1977).
[11] M. J. Kim and T. R. Powers, Phys. Rev. E **69**, 061910 (2004).
[12] M. Reichert and H. Stark, Eur. Phys. J. E **17**, 493 (2005).
[13] G. J. Elfring and E. Lauga, Phys. Rev. Lett. **103**, 088101 (2009).
[14] B. Qian, H. Y. Jiang, D. A. Gagnon, K. S. Breuer, and T. R. Powers, Phys. Rev. E **80**, 061919 (2009).
[15] J. Kotar, M. Leoni, B. Bassetti, M. C. Kagomarsino, and P. Cicuta, P. Natl. Acad. Sci. USA **107**, 7669 (2010).
[16] M. Kim, J. C. Bird, A. J. Van Parijs, K. S. Breuer, and T. R. Powers, P. Natl. Acad. Sci. USA **100**, 15482 (2003).
[17] H. Flores, E. Lobaton, S. Méndez-Diez, S. Tlupova, and R. Cortez, B. Math. Biol. **67**, 137 (2005).
[18] N. Watari and R. G. Larson, Biophys. J. **98**, 12 (2010).
[19] N. C. Darnton and H. C. Berg, Biophys. J. **92**, 2230 (2007).
[20] H. Wada and R. R. Netz, Eur. Phys. Lett. **82**, 28001 (2008).
[21] R. Vogel and H. Stark, Eur. Phys. J. E **33**, 259 (2010).
[22] H. C. Berg and L. Turner, Biophys. J. **65**, 2201 (1993).
[23] X. Chen and H. C. Berg, Biophys. J. **78**, 10361041 (2000).
[24] H. C. Berg and R. A. Anderson, Nature **245**, 380 (1977).
[25] L. Turner, W. S. Ryu, and H. C. Berg, J. Bacteriol. **182**, 2793 (2000).
[26] N. C. Darnton, L. Turner, S. Rojevsky, and H. C. Berg, J. Bacteriol. **189**, 1756 (2007).

[27] C. F. Schmid, L. H. Switzer, and D. J. Klingenberg, J. Rheol. **44**, 781 (2000).
[28] S. Kim and S. J. Karrila, *Microhydrodynamics: Principles and Selected Applications* (Dover Publications, Inc., Mineola, NY, 2005).
[29] J. P. Hernandez-Ortiz, J. J. de Pablo, and M. D. Graham, Phys. Rev. Lett. **98**, 140602 (2007).
[30] R. R. Sundararajakumar and D. L. Koch, J. Non-Newtonian Fluid Mech. **73**, 205 (1997).
[31] M. Fujii, S. Shibata, and S. I. Aizawa, J. Mol. Biol. **379**, 273 (2008).
[32] G. M. Garrity, D. J. Brenner, N. R. Krieg, and J. R. Staley, *Bergey's Manual of Systematic Bacteriology, Volume Two: The Proteobacteria* (Springer-Verlag, New York, 2008).
[33] L. Turner, R. Zhang, N. C. Darnton, and H. C. Berg, J. Bacteriol. **192**, 3259 (2010).
[34] H. C. Berg, Ann. Rev. Biochem. **72**, 19 (2003).
[35] T. Mora, H. Yu, and N. S. Wingreen, Phys. Rev. Lett. **103**, 248102 (2009).